PERGAMON

International Journal of Solids and Structures 37 (2000) 1251–1274

INTERNATIONAL JOURNAL OF SOLIDS and STRUCTURES

www.elsevier.com/locate/ijsolstr

Cracks problem for non-homogeneous composite material subjected to dynamic loading

B.L. Wang*, J.C. Han, S.Y. Du

Center for Composite Materials, Harbin Institute of Technology, Harbin 150001, People's Republic of China

Received 9 July 1997; in revised form 28 September 1998

Abstract

In this paper, we present a method to analyse the dynamic and steady response of non-homogeneous composite materials. Differing from the existing works reported in literature, the present method can be used for arbitrarily varying material properties through thickness direction and the crack number can be larger than one. It is assumed that the composite material is orthotropic and all the material properties depend only on the coordinates y (along the thickness direction). The material non-homogeneity is simulated by dividing the plate into a number of layers, each layer is assigned slightly different material properties. The method is based upon the Fourier and Laplace transforms to reduce the boundary value problem to a system of generalized singularity integral equations in the Laplace transform domain. The singular integral equations for the problem are derived and numerically solved by weighted residual value methods. By utilized numerical Laplace inversion the time-dependent full field solutions are obtained. As the numerical illustrates, three different cracked specimens, a functionally graded material, a metal-ceramic joint with functionally graded interlayer, and a metal substrate/functionally graded film structure are presented for various material non-homogeneity parameters and/or functionally graded layer thickness. The results obtained demonstrate that the present model is an efficient tool in the fracture analysis of composite materials with properties varying in the thickness direction.

1. Introduction

Non-homogeneous composites are of considerable technical and engineering importance. These materials have properties that vary as a function of position in the body. Composite materials such as Functionally Graded Materials (FGMs) have continuously varying properties. Other classes of materials such as laminates possess non-homogeneity of discontinuous nature. The material properties in one lamina may be different from another although each of the lamina may still be homogeneous.

* Corresponding author. Fax: 0086-451-622-1048.
E-mail address: wangbl@public.hr.hl.cn (B.L. Wang).

0020-7683/00/$ - see front matter
PII: S0020-7683(98)00292-3

There are uncertainties arising from voids and defects that are introduced in the composite during manufacturing. Even a small quantity of mechanical imperfections can cause a marked influence on the composite strength. The fracture mechanical analysis, especially the dynamic fracture analysis of the non-homogeneous material with multi-cracks is necessary. Analysis of the overall mechanical properties of the non-homogeneous composites has been developed to an advanced level. But when fracture of these materials is investigated and exact strongly non-uniform stress distribution is required, the non-homogeneity essentially complicates the analysis. For composites with continuously varying material properties, it is often conventional to take the properties to be some certain assumed functions of space variable, for examples, exponential functions (Erdogan, 1985; Delale and Erdogan, 1988a, b; Ozturk and Erdogan, 1993, 1995, 1996), power-law type functions (Hata, 1985). Such idealizations offer considerable amount of simplifications to the analysis and leads to the system differential equations remaining formally the same with constant coefficients. But Zuiker has pointed out that certain assumed property distributions presented in the literature must be used with care as they are not physically realizable for certain material distributions (Zuiker, 1995). For composites with discontinuous varying materials properties such as multi-layers, an approximate discrete model was employed to study the steady state crack propagation (Slepyan, 1974). Another way to avoid difficulties arising in the study of fracture of the multilayered laminates is to use models with a reduced number of layers (Chen and Sih, 1971; Ashbaugh, 1973). In that work multilayered composite is replaced by a three-layered system where the cracked layer of one material is sandwiched between two half-spaces of the second material. Employing for such models with a reduced number of layers is possible only in the special case of 'short' loading when the characteristic layer thickness sufficiently exceeds the length parameter associated with the load distribution (Ryvkin, 1996).

An investigation of the stress field near the crack tip in a multilayered composite consisting of layers with the ratio of the crack length to the characteristic layer thickness is not too small leads to the necessity of introducing models with a large number of layers. For materials with properties continuously varying but not according to exponential law or power-law, a new model is necessary. In this paper, we first divided the elastic region into a number of layers of infinite length and the material properties are taken to be constants for each layer, then utilizing the Laplace transform and Fourier transform technique to get the general solutions of the displacements for each layer. The complete solution of the entire elastic region is then obtained through introducing layer interface conditions and the mechanical boundary condition via the flexibility/stiffness matrix approach. Attention is focused on the time-dependent full field solutions of stress, stress intensity factor and strain energy release rate. As the numerical illustrations, the dynamic stress intensity factors for three different cracked specimens with functionally graded layer under sudden applied stress on crack faces are presented for various material non-homogeneous parameters and graded layer thickness.

2. Formulation of the problem

Consider a non-homogeneous material of height h with properties that vary as a function of coordinate y (Fig. 1). The length of x-direction is infinite. (x, y, z) is global coordinate system. In order to simulate material non-homogeneity in y-direction, divide the elastic plate into N layer elements of infinite length (for laminate, each layer may be further divided into some sub-layers). The material properties are taken to be constant for each layer. The main axes of elasticity are parallel to x-axis and y-axis. For the Jth strip, the density is ρ_J, thickness is h_J (throughout the paper the subscript J is associated with the Jth layer, counted up from the lower surface, the subscript j denotes the interface number between the Jth layer and the $(J+1)$th layer). The local coordinate system (x_J, y_J, z_J) is related to global coordinate by:

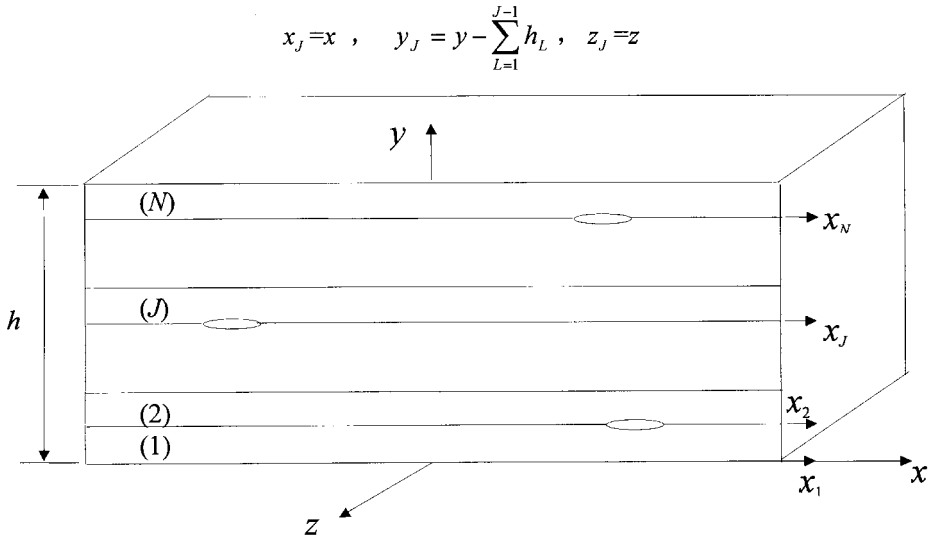

Fig. 1. The geometry and coordinates of non-homogeneous composite plate.

$$x_J = x, \quad y_J = y - \sum_{L=1}^{J-1} h_L, \quad z_J = z. \tag{1}$$

Denote the interlamina stress $(\sigma_y)_j$ and $(\tau_{xy})_j$ as $\sigma_j(x, t)$ and $\tau_j(x, t)$. The adjacent two layers are perfectly bonded or with a crack. The crack length is $2a_j$, crack center locate in the position of $x_j = c_j$. The initial displacement and velocity are zero, the boundary conditions are:

1. The applied stresses in crack faces are

$$\sigma_j(x, t) = \sigma_{0j}(x, t) \quad \tau_j(x, t) = \tau_{0j}(x, t) \quad c_j - a_j < x < c_j + a_j. \tag{2}$$

2. The stress on upper and lower surface of the composite plate are zero.
3. The stress and displacement is zero at infinity.

Under plane strain, for orthotropic material, the only non-zero displacement and stress field is

$$(U_x)_J = u_J(x, y_J, t) \; (U_y)_J = v_J(x, y_J, t) \tag{3a}$$

$$(\sigma_x)_J = (C_{11})_J \frac{\partial u_J}{\partial x} + (C_{12})_J \frac{\partial v_J}{\partial y_J}$$

$$(\sigma_y)_J = (C_{12})_J \frac{\partial u_J}{\partial x} + (C_{22})_J \frac{\partial v_J}{\partial y_J}$$

$$(\tau_{xy})_J = (C_{66})_J \left(\frac{\partial u_J}{\partial y_J} + \frac{\partial v_J}{\partial x} \right) \tag{3b}$$

where $(C_{mn})_J$ $(m, n = 1, 2, 6)$ are stiffness coefficients for the Jth layer. Under small deformation, the equation of motion requires the satisfaction of the following wave equation

$$(C_{11})_J\frac{\partial^2 u_J}{\partial x^2}+(C_{66})_J\frac{\partial^2 u_J}{\partial y_J^2}+(C_{12}+C_{66})_J\frac{\partial^2 v_J}{\partial x\partial y_J}=\rho_J\frac{\partial^2 u_J}{\partial t^2}$$

$$(C_{66})_J\frac{\partial^2 v_J}{\partial x^2}+(C_{22})_J\frac{\partial^2 v_J}{\partial y_J^2}+(C_{12}+C_{66})_J\frac{\partial^2 u_J}{\partial x\partial y_J}=\rho_J\frac{\partial^2 v_J}{\partial t^2}. \tag{4a}$$

Referring to the following non-dimensional variable

$$\bar{x}=x/h\quad \bar{y}_J=y_J/h\quad \bar{h}_J=h_J/h\quad \bar{a}_j=a_j/h\quad \bar{c}_j=c_j/h \tag{4b}$$

and the wave velocity:

$$C_{aJ}=\sqrt{(C_{22})_J/\rho_J}\quad C_{bJ}=\sqrt{(C_{66})_J/\rho_J}. \tag{4c}$$

Applying the Laplace transform over the time variable t, from (4a), we have

$$\left(\frac{C_{11}}{C_{66}}\right)_J\frac{\partial^2 u_J^*}{\partial\bar{x}^2}+\frac{\partial^2 u_J^*}{\partial\bar{y}_J^2}+\left(1+\frac{C_{12}}{C_{66}}\right)_J\frac{\partial^2 v_J^*}{\partial\bar{x}\,\partial\bar{y}_J}=\left(\frac{ph}{C_{bJ}}\right)^2 u_J^*$$

$$\left(\frac{C_{66}}{C_{22}}\right)_J\frac{\partial^2 v_J^*}{\partial\bar{x}^2}+\frac{\partial^2 v_J^*}{\partial\bar{y}_J^2}+\left(\frac{C_{66}+C_{12}}{C_{22}}\right)_J\frac{\partial^2 u_J^*}{\partial\bar{x}\,\partial\bar{y}_J}=\left(\frac{ph}{C_{aJ}}\right)^2 v_J^* \tag{4d}$$

where the superscript * denotes the Laplace transform with the parameter of the transformation denoted by p. Using Fourier transform to the space variable x, eqn (4d) may be solved to give the displacement in each layer of the material:

$$\begin{Bmatrix} u_J^*(\bar{x},\bar{y}_J,p) \\ \underline{v_J^*(\bar{x},\bar{y}_J,p)} \\ i \end{Bmatrix}=\frac{h}{2\pi}\int_{-\infty}^{+\infty}\left[e_J(\bar{y}_J,p)\right]\begin{Bmatrix} A_{1J}(s,p) \\ B_{1J}(s,p) \\ A_{2J}(s,p) \\ B_{2J}(s,p) \end{Bmatrix}\mathrm{e}^{-is\bar{x}}\,\mathrm{d}s. \tag{5a}$$

In which A_{1J}, B_{1J}, A_{2J}, B_{2J} are unknowns to be determined, $i=\sqrt{-1}$,

$$\left[e_J(\bar{y}_J,\ p)\right]=\begin{bmatrix} \mathrm{e}^{-S\lambda_{1J}\bar{y}_J} & \mathrm{e}^{S\lambda_{1J}\bar{y}_J} & \mathrm{e}^{-S\lambda_{2J}\bar{y}_J} & \mathrm{e}^{S\lambda_{2J}\bar{y}_J} \\ -\eta_{1J}\,\mathrm{e}^{-S\lambda_{1J}\bar{y}_J} & \eta_{1J}\,\mathrm{e}^{S\lambda_{1J}\bar{y}_J} & -\eta_{2J}\,\mathrm{e}^{-S\lambda_{2J}\bar{y}_J} & \eta_{2J}\mathrm{e}^{S\lambda_{2J}\bar{y}_J} \end{bmatrix}, \tag{5b}$$

and, λ_{iJ} $(i=1,2)$ are the roots of the following characteristic equation:

$$\begin{aligned}\lambda_{iJ}^4-&\left[\left(\frac{C_{11}C_{22}-2C_{12}C_{66}-C_{12}^2}{C_{22}C_{66}}\right)_J+\left(\frac{ph}{sC_{aJ}}\right)^2+\left(\frac{ph}{sC_{bJ}}\right)^2\right]\lambda_{iJ}^2\\&+\left[\left(\frac{C_{11}}{C_{22}}\right)_J+\left(\frac{ph}{sC_{aJ}}\right)^2\right]\left[1+\left(\frac{ph}{sC_{bJ}}\right)^2\right]=0,\end{aligned} \tag{5c}$$

while $\eta_{iJ}(i=1,2)$ are:

$$\eta_{iJ}=\frac{(C_{11})_J/(C_{66})_J+(ph/sC_{bJ})^2-\lambda_{iJ}^2}{\lambda_{iJ}\left(1+(C_{12})_J/(C_{66})_J\right)}. \tag{5d}$$

Substitution of eqn (5a) into (3b) gives the stress $(\sigma_j^*(\bar{x},p),\ \tau_j^*(\bar{x},p))$ at $(\bar{y}_J=\bar{h}_J)$ and $(\sigma_{j-1}^*(\bar{x},p),\ \tau_{j-1}^*(\bar{x},p))$ at $(\bar{y}_J=0)$:

$$\begin{Bmatrix} \sigma_j^*(\bar{x},p)/i \\ \tau_j^*(\bar{x},p) \\ \sigma_{j-1}^*(\bar{x},p)/i \\ \tau_{j-1}^*(\bar{x},p) \end{Bmatrix} = \frac{1}{2\pi}\int_{-\infty}^{+\infty} s\big[K_J(s,p)\big] \begin{Bmatrix} A_{1J}(s,p) \\ B_{1J}(s,p) \\ A_{2J}(s,p) \\ B_{2J}(s,p) \end{Bmatrix} \mathrm{e}^{-is\bar{x}}\,\mathrm{d}s \tag{6a}$$

where

$$\big[K_J(s,p)\big] = \begin{bmatrix} \big(\lambda_{1J}\eta_{1J}(C_{22})_J-(C_{12})_J\big)\,\mathrm{e}^{-s\lambda_{1J}\bar{h}_J} & \big(\lambda_{1J}\eta_{1J}(C_{22})_J-(C_{12})_J\big)\,\mathrm{e}^{s\lambda_{1J}\bar{h}_J} \\ \big(-\lambda_{1J}-\eta_{1J}\big)(C_{66})_J\,\mathrm{e}^{-s\lambda_{1J}\bar{h}_J} & \big(\lambda_{1J}+\eta_{1J}\big)(C_{66})_J\,\mathrm{e}^{s\lambda_{1J}\bar{h}_J} \\ \lambda_{1J}\eta_{1J}(C_{22})_J-(C_{12})_J & \lambda_{1J}\eta_{1J}(C_{22})_J-(C_{12})_J \\ \big(-\lambda_{1J}-\eta_{1J}\big)(C_{66})_J & \big(\lambda_{1J}+\eta_{1J}\big)(C_{66})_J \\ \big(\lambda_{2J}\eta_{2J}(C_{22})_J-(C_{12})_J\big)\,\mathrm{e}^{-s\lambda_{2J}\bar{h}_J} & \big(\lambda_{2J}\eta_{2J}(C_{22})_J-(C_{12})_J\big)\,\mathrm{e}^{s\lambda_{2J}\bar{h}_J} \\ \big(-\lambda_{2J}-\eta_{2J}\big)(C_{66})_J\,\mathrm{e}^{-s\lambda_{2J}\bar{h}_J} & \big(\lambda_{2J}+\eta_{2J}\big)(C_{66})_J\,\mathrm{e}^{s\lambda_{2J}\bar{h}_J} \\ \lambda_{2J}\eta_{2J}(C_{22})_J-(C_{12})_J & \lambda_{2J}\eta_{2J}(C_{22})_J-(C_{12})_J \\ \big(-\lambda_{2J}-\eta_{2J}\big)(C_{66})_J & \big(\lambda_{2J}+\eta_{2J}\big)(C_{66})_J \end{bmatrix} \tag{6b}$$

$$\big[K_J(s,p)\big]^{-1} = \big[D_J^a(s,p), D_J^a(s,p)\big] \tag{6c}$$

in which $[D_J^a(s,p)]$ and $[D_J^b(s,p)]$ are matrices having four rows and two columns each. Applying inverse Fourier transform to (6a) yields $(A_{1J}, B_{1J}, A_{2J}, B_{2J})$ in terms of vector $(\sigma_j^*, \tau_j^*, \sigma_{j-1}^*, \tau_{j-1}^*)$. The displacements in each layer can thus be determined in terms of $(\sigma_j^*, \tau_j^*, \sigma_{j-1}^*, \tau_{j-1}^*)$ by substituting $(A_{1J}, B_{1J}, A_{2J}, B_{2J})$ back into (5a)

$$\begin{Bmatrix} u_J^*\big(\bar{r},\bar{y}_J,p\big) \\ \dfrac{v_J^*\big(\bar{r},\bar{y}_J,p\big)}{i} \end{Bmatrix} = \frac{h}{2\pi}\int_{-\infty}^{+\infty}\frac{1}{s}\big[e_J\big(\bar{y}_J,p\big)\big]\Big(\big[D_J^a(s,p)\big]\big[D_J^b(s,p)\big]\Big)$$

$$\left\{\int_{-\infty}^{+\infty}\frac{\sigma_j^*(\bar{x},p)}{i}\,\mathrm{e}^{is\bar{x}}\mathrm{d}\bar{x}\int_{-\infty}^{+\infty}\tau_j^*(\bar{x},p)\,\mathrm{e}^{is\bar{x}}\mathrm{d}\bar{x}\int_{-\infty}^{+\infty}\frac{\sigma_{j-1}^*(\bar{x},p)}{i}\mathrm{e}^{is\bar{x}}\mathrm{d}\bar{x}\right.$$
$$\left.\int_{-\infty}^{+\infty}\tau_{j-1}^*(\bar{x},p)\,\mathrm{e}^{is\bar{x}}\mathrm{d}\bar{x}\right\}^{\mathrm{T}}\mathrm{e}^{-is\bar{r}}\,\mathrm{d}s. \tag{7}$$

3. Singular integral equations

By introducting the following dislocation density function

$$\phi_{xj}(\bar{x},p)=\frac{\partial u^*_{J+1}(\bar{x},\bar{y}_{j+1}=0,p)}{\partial x}-\frac{\partial u^*_J(\bar{x},\bar{y}_J=\bar{h}_J,p)}{\partial x}$$

$$\phi_{yj}(\bar{x},p)=\frac{\partial v^*_{J+1}(\bar{x},\bar{y}_{j+1}=0,p)}{\partial x}-\frac{\partial v^*_J(\bar{x},\bar{y}_J=\bar{h}_J,p)}{\partial x}. \tag{8}$$

Under the single-valueness of the displacement along the interface, if the interface between the Jth and the $(J+1)$th layer is perfectly bonded then ϕ_{xj} and ϕ_{yj} are zeros, if there is a crack between the Jth and the $(J+1)$th layer then

$$\phi_{xj}(\bar{x},p)=\phi_{yj}(\bar{x},p)=0 \quad \bar{x}>\bar{c}_j+\bar{a}_j \quad \text{or } \bar{x}<\bar{c}_j-\bar{a}_j \tag{9a}$$

$$\int_{\bar{c}_j-\bar{a}_j}^{\bar{c}_j+\bar{a}_j}\phi_{xj}(\bar{x},p)\,\mathrm{d}\bar{x}=\int_{\bar{c}_j-\bar{a}_j}^{\bar{c}_j+\bar{a}_j}\phi_{yj}(\bar{x},p)\,\mathrm{d}\bar{x}=0. \tag{9b}$$

Substituting of (7) into (8) gives

$$\begin{Bmatrix}\phi_{xj}(\bar{r},p)\\ \phi_{yj}(\bar{r},p)/i\end{Bmatrix}=\frac{1}{2\pi}\int_{-\infty}^{+\infty}\begin{pmatrix}[L]_j & [M]_j & [N]_j\end{pmatrix}\mathrm{e}^{-is\bar{r}}\,\mathrm{d}s$$

$$\times\int_{-\infty}^{+\infty}\begin{Bmatrix}\sigma^*_{j-1}(\bar{x}) & i\tau^*_{j-1}(\bar{x}) & \sigma^*_j(\bar{x}) & i\tau^*_j(\bar{x}) & \sigma^*_{j+1}(\bar{x}) & i\tau^*_{j+1}(\bar{x})\end{Bmatrix}^{\mathrm{T}}\mathrm{e}^{is\bar{x}}\,\mathrm{d}\bar{x} \tag{10a}$$

where

$$[L(s,p)]_j=[e_J(\bar{h}_J,p)][D^b_J(s,p)],\quad [N(s,p)]_j=-[e_{J+1}(0,p)][D^a_{J+1}(s,p)],$$

$$[M(s,p)]_j=[e_J(\bar{h}_J,p)][D^a_J(s,p)]-[e_{J+1}(0,p)][D^b_{J+1}(s,p)]. \tag{10b}$$

The Fourier transform of (10a) gives

$$\begin{pmatrix}[L]_j & [M]_j & [N]_j\end{pmatrix}\int_{-\infty}^{+\infty}\begin{Bmatrix}\sigma^*_{j-1}(\bar{x}) & i\tau^*_{j-1}(\bar{x}) & \sigma^*_j(\bar{x}) & i\tau^*_j(\bar{x}) & \sigma^*_{j+1}(\bar{x}) & i\tau^*_{j+1}(\bar{x})\end{Bmatrix}^{\mathrm{T}}\mathrm{e}^{is\bar{x}}\,\mathrm{d}\bar{x}$$

$$=\int_{\bar{c}_j-\bar{a}_j}^{\bar{c}_j+\bar{a}_j}\begin{Bmatrix}\phi_{xj}(\bar{r},p)\\ \phi_{yj}(\bar{r},p)/i\end{Bmatrix}\mathrm{e}^{is\bar{r}}\,\mathrm{d}\bar{r}. \tag{10c}$$

Defining the following two vectors of $2(N-1)$ rows each

$$\{\Phi(s,p)\}=\left\{\int_{\bar{c}_1-\bar{a}_1}^{\bar{c}_1+\bar{a}_1}\phi_{x1}\,\mathrm{e}^{is\bar{r}}\,\mathrm{d}\bar{r}\quad\int_{\bar{c}_1-\bar{a}_1}^{\bar{c}_1+\bar{a}_1}\frac{\phi_{y1}}{i}\,\mathrm{e}^{is\bar{r}}\,\mathrm{d}\bar{r},\ldots,\int_{\bar{c}_{N-1}-\bar{a}_{N-1}}^{\bar{c}_{N-1}+\bar{a}_{N-1}}\phi_{x(N-1)}\,\mathrm{e}^{is\bar{r}}\,\mathrm{d}\bar{r}\right.$$

$$\left.\int_{\bar{c}_{N-1}-\bar{a}_{N-1}}^{\bar{c}_{N-1}+\bar{a}_{N-1}}\frac{\phi_{y(N-1)}}{i}\,\mathrm{e}^{is\bar{r}}\,\mathrm{d}\bar{r}\right\}^{\mathrm{T}}$$

$$\{T(\bar{x},p)\} = \{\sigma_1^* \quad i\tau_1^* \quad ,\ldots, \quad \sigma_{N-1}^* \quad i\tau_{N-1}^*\}^{\mathrm{T}}, \tag{11}$$

and utilizing the traction free condition of the exterior surface of the composite plate, from (10c) we have

$$[D(s,p)]\int_{-\infty}^{+\infty}\{T(\bar{x},p)\}\,\mathrm{e}^{is\bar{x}}\,\mathrm{d}\bar{x} = \{\Phi(s,p)\}. \tag{12a}$$

In which, the flexibility matrix $[D(s,p)]$ and its inversion (i.e. the stiffness matrix $K(s,p)$) are

$$[D(s,p)] = \begin{bmatrix} M_1 & N_1 & & & & \\ L_2 & M_2 & N_2 & & & \\ & & \ddots & & & \\ & & & L_{N-2} & M_{N-2} & N_{N-2} \\ & & & & L_{N-1} & M_{N-1} \end{bmatrix}, \quad [D(s,p)]^{-1} = [K(s,p)]. \tag{12b}$$

Applying the inverse Fourier transform to (12a) yields

$$\{T(\bar{x},p)\} = \frac{1}{2\pi}\int_{-\infty}^{+\infty}[K(s,p)]\Phi(s,p)\,\mathrm{e}^{-is\bar{x}}\,\mathrm{d}s. \tag{13}$$

This is the relationship between interfacial stress and dislocation density function, and there are $2(N-1)$ equations in it. For those interfaces with no crack, the dislocation density function is zero, so the number of equations needed to be solved is twice the crack number. Referring to variable $K_m^n(s,p)$, which denote the mth row and the nth column in matrix $[K(s,p)]$, one can rewrite (13) as

$$\begin{Bmatrix} \sigma_j^*(\bar{x},p) \\ i\tau_j^*(\bar{x},p) \end{Bmatrix} = \frac{1}{2\pi}\sum_{k=1}^{N-1}\int_{\bar{c}_k-\bar{a}_k}^{\bar{c}_k+\bar{a}_k}\left(\int_{-\infty}^{+\infty}\begin{bmatrix} K_{(2j-1)}^{(2k-1)}(s,p) & K_{(2j-1)}^{(2k)}(s,p) \\ K_{(2j)}^{(2k-1)}(s,p) & K_{(2j)}^{(2k)}(s,p) \end{bmatrix}\mathrm{e}^{is(\bar{r}-\bar{x})}\,\mathrm{d}s\right)\begin{Bmatrix} \phi_{xk}(\bar{r}) \\ \phi_{yk}(\bar{r})/i \end{Bmatrix}\mathrm{d}\bar{r}. \tag{14}$$

To investigate and to separate a singular part of the kernel in (14), the asymptotic behavior of the elements in matrix $[K(s,p)]$ for $|s|\to\infty$ must be examined. For the interface with no crack, since the dislocation density function is zero, one only needs to analyze the elements related to the cracked interfaces. If material properties are not continuous along the cracked plane, the local stress behave in an oscillatory nature which leads to interpenetrating of material points of the crack surface (Williams, 1959), such a condition cannot be realized physically and is outside the scope of this paper. We only consider the special case of continuously varying material properties along the cracked plane (however, the material properties may not be continuous along the uncracked interface).

As $|s|\to\infty$ the only non-zero elements in $[K(s,p)]$ are

$$K_{(2j-1)}^{(2j)}(\infty,p) = \lim_{s\to\pm\infty}K_{(2j-1)}^{(2j)}(s,p) = \frac{\mathrm{sgn}(s)}{2}\left(G_y\right)_j \tag{15a}$$

$$K_{(2j)}^{(2j-1)}(\infty,p) = \lim_{s\to\pm\infty}K_{(2j)}^{(2j-1)}(s,p) = \frac{\mathrm{sgn}(s)}{2}(G_x)_j \tag{15b}$$

where

$$(G_x)_j = \frac{\left((C_{11})_J + (C_{12})_J\lambda_{1J}{}^2\right)\left((C_{11})_J + (C_{12})_J\lambda_{2J}{}^2\right)(C_{66})_J}{(C_{11})_J\left((C_{12})_J + (C_{66})_J\right)(\lambda_{1J} + \lambda_{2J})}, \quad \left(G_y\right)_j = \frac{(G_x)_j}{\lambda_{1J}\lambda_{2J}} \tag{15c}$$

in which λ_{1J}, λ_{2J} are roots of characteristic eqn (5c) in the case of $|s| \to \infty$

By defining $\bar{k}^n_m(s,p) = k^n_m(s,p) - k^n_m(\infty,p)$ and employing the Fourier representation of a generalized function (Gradshteyn and Ryzhik, 1965)

$$\int_{-\infty}^{+\infty} \frac{\mathrm{sgn}(s)}{2} \mathrm{e}^{is(\bar{r}-\bar{x})}\,\mathrm{d}s = \frac{i}{(\bar{r}-\bar{x})}, \tag{16}$$

one can express (14) as follows

$$\begin{Bmatrix} \sigma^*_j(\bar{x},p) \\ i\tau^*_j(\bar{x},p) \end{Bmatrix} = \frac{1}{2\pi}\sum_{k=1}^{N-1}\int_{\bar{c}_k-\bar{a}_k}^{\bar{c}_k+\bar{a}_k}\left(\int_{-\infty}^{+\infty}\begin{bmatrix} \bar{k}^{(2k-1)}_{(2j-1)}(s,p) & \bar{k}^{(2k)}_{(2j-1)}(s,p) \\ \bar{k}^{(2k-1)}_{(2j)}(s,p) & \bar{k}^{(2k)}_{(2j)}(s,p) \end{bmatrix}\mathrm{e}^{is(\bar{r}-\bar{x})}\,\mathrm{d}s\right)\begin{Bmatrix} \phi_{xk}(\bar{r}) \\ \phi_{yk}(\bar{r}/i) \end{Bmatrix}\mathrm{d}\bar{r}$$
$$+\begin{Bmatrix} \dfrac{\left(G_y\right)_j}{2\pi}\displaystyle\int_{\bar{c}_j-\bar{a}_j}^{\bar{c}_j+\bar{a}_j}\dfrac{\phi_{yj}(\bar{r})}{\bar{r}-\bar{x}}\,\mathrm{d}\bar{r} \\ \dfrac{(G_x)_j}{2\pi}\displaystyle\int_{\bar{c}_j-\bar{a}_j}^{\bar{c}_j+\bar{a}_j}\dfrac{\phi_{xj}(\bar{r})i}{\bar{r}-\bar{x}}\,\mathrm{d}\bar{r} \end{Bmatrix}. \tag{17}$$

As $\bar{k}^n_m(s,p)$ is odd function of s when $m+n$ equal odd number, and even function of s when $m+n$ equal even number. Eqn (17) may be further simplified to

$$\begin{Bmatrix} \sigma^*_j(\bar{x},p) \\ \tau^*_j(\bar{x},p) \end{Bmatrix} = \frac{1}{\pi}\sum_{k=1}^{N-1}\int_{\bar{c}_k-\bar{a}_k}^{\bar{c}_k+\bar{a}_k}\left(\int_{0}^{+\infty}\begin{bmatrix} \bar{k}^{(2k-1)}_{(2j-1)}(s,p)\cos s(\bar{r}-\bar{x}) & \bar{k}^{(2k)}_{(2j-1)}(s,p)\sin s(\bar{r}-\bar{x}) \\ \bar{k}^{(2k-1)}_{(2j)}(s,p)\sin s(\bar{r}-\bar{x}) & -\bar{k}^{(2k)}_{(2j)}(s,p)\cos s(\bar{r}+\bar{x}) \end{bmatrix}\mathrm{d}s\right)\begin{Bmatrix} \phi_{xk}(\bar{r}) \\ \phi_{yk}(\bar{r}) \end{Bmatrix}\mathrm{d}\bar{r} \tag{18}$$

$$+\begin{Bmatrix} \dfrac{\left(G_y\right)_j}{2\pi}\displaystyle\int_{\bar{c}_j-\bar{a}_j}^{\bar{c}_j+\bar{a}_j}\dfrac{\phi_{yj}(\bar{r})}{\bar{r}-\bar{x}}\,\mathrm{d}\bar{r} \\ \dfrac{(G_x)_j}{2\pi}\displaystyle\int_{\bar{c}_j-\bar{a}_j}^{\bar{c}_j+\bar{a}_j}\dfrac{\phi_{xj}(\bar{r})i}{\bar{r}-\bar{x}}\,\mathrm{d}\bar{r} \end{Bmatrix}.$$

Referring to the following non-dimensional parameters

$$\bar{r}_j = \left(\bar{r}-\bar{c}_j\right)/\bar{a}_j \quad \bar{x}_j = \left(\bar{x}-\bar{c}_j\right)/\bar{a}_j \tag{19a}$$

$$\varphi_{xj}\left(\bar{r}_j,p\right) = \phi_{xj}\left(\bar{a}_j\bar{r}_j+\bar{c}_j,p\right) \quad \varphi_{yj}\left(\bar{r}_j,p\right) = \phi_{yj}\left(\bar{a}_j\bar{r}_j+\bar{c}_j,p\right) \tag{19b}$$

$$\left[h_{jk}\left(p,\bar{r}_k,\bar{x}_j\right)\right] = \bar{a}_k\int_0^{+\infty}\begin{bmatrix} \bar{k}^{(2k-1)}_{(2j-1)}(s,p)\cos s(\bar{r}-\bar{x}) & \bar{k}^{(2k)}_{(2j-1)}(s,p)\sin s(\bar{r}-\bar{x}) \\ \bar{k}^{(2k-1)}_{(2j)}(s,p)\sin s(\bar{r}-\bar{x}) & -\bar{k}^{(2k)}_{(2j)}(s,p)\cos s(\bar{r}+\bar{x}) \end{bmatrix}\mathrm{d}s. \tag{19c}$$

Eqn (18) may be re-written as

$$\begin{Bmatrix} \sigma_j^*(\bar{x}, p) \\ \tau_j^*(\bar{x}, p) \end{Bmatrix} = \frac{1}{\pi}\sum_{k=1}^{N-1}\int_{-1}^{1}\left[h_{jk}(p, \bar{r}_k, \bar{x}_j)\right]\begin{Bmatrix} \varphi_{xk}(\bar{r}_k) \\ \varphi_{yk}(\bar{r}_k) \end{Bmatrix} \mathrm{d}\bar{r}_k + \begin{Bmatrix} \dfrac{(G_y)_j}{2\pi} & \displaystyle\int_{-1}^{1} \dfrac{\varphi_{yj}(\bar{r}_j)}{\bar{r}_j - \bar{x}_j}\,\mathrm{d}\bar{r}_j \\ \dfrac{(G_x)_j}{2\pi} & \displaystyle\int_{-1}^{1} \dfrac{\varphi_{xj}(\bar{r}_j)}{\bar{r}j - \bar{x}_j}\,\mathrm{d}\bar{r}_j \end{Bmatrix}. \tag{20}$$

The integral $\lfloor h_{jk}(\bar{r}_k, \bar{x}_j)\rfloor$ is a Fredholm kernel which is bounded for all values of $\bar{r}_k$ and $\bar{x}_j$ in the closed interval $[-1, 1]$.

4. Solution of the singular integral equations

It can be seen that eqn (20) provides the expression for (σ_j^*,τ_j^*) outside as well as inside the crack. In the case of inside the crack, it is an ordinary sigular integral equation having a simple Cauchy-type kernel $1/(\bar{r}_j - \bar{x}_j)$ as the dominant singular part. With the Cauchy-type kernel in (20) being the sole contribution to the dislocation density functions $\varphi_{xj}(\bar{r}_j, p)$ and $\varphi_{yj}(\bar{r}_j, p)$, the crack-tip behavior can be characterized by standard square-root singular such that (Muskhelishvili, 1953)

$$\varphi_{xj}(\bar{r}_j, p) = g_{xj}(\bar{r}_j, p)/\sqrt{1-\bar{r}_j^2}, \quad \varphi_{yj}(\bar{r}_j, p) = g_{yj}(\bar{r}_j, p)/\sqrt{1-\bar{r}_j^2}. \tag{21}$$

The integral eqn (20) is thus solved numerically by noting that its fundamental function corresponds to the weight function of the Chebyshev polynomial of the first kind $T_m(\bar{r}_j)$. The unknown functions (g_{xj}, g_{yj}) can therefore be expressed as

$$(g_{xj}, g_{yj}) = \sum_{m=1}^{\infty}\left(C_{jm}^{x}(p), C_{jm}^{y}(p)\right)T_m(\bar{r}_j) \tag{22}$$

where $(C_{jm}^{x}(p), C_{jm}^{y}(p))$ are the unknowns to be evaluated. It is observed that the compatibility condition (9b) is identically satisfied by the above expansion. After substituting (22), truncated with the first M terms in it, into (20) and using the integral formulas (Gradshteyn and Ryzhik, 1965)

$$\frac{1}{\pi}\int_{-1}^{1}\frac{T_m(\bar{r}_j)}{(\bar{r}_j - \bar{x}_j)\sqrt{1-\bar{r}_j^2}}\,\mathrm{d}\bar{r}_j = \begin{cases} U_{m-1}(\bar{x}_j) & m \geqslant 1 \quad |\bar{x}_j| < 1 \\ -\dfrac{\mathrm{sgn}(\bar{x}_j)}{\sqrt{\bar{x}_j^2-1}}\left[\bar{x}_j - \mathrm{sgn}(\bar{x}_j)\sqrt{\bar{x}_j^2-1}\right]^m & m \geqslant 0 \quad |\bar{x}_j| > 1, \\ 0 & m = 0 \quad |\bar{x}_j| < 1 \end{cases} \tag{23}$$

we have

$$\begin{Bmatrix} \sigma_j^*(\bar{a}_j\bar{x}_j + \bar{c}_j, p) \\ \tau_j^*(\bar{a}_j\bar{x}_j + \bar{c}_j, p) \end{Bmatrix} = \sum_{k=1}^{N-1}\sum_{m=1}^{M}\left[V_j^{km}(\bar{x}_j)\right]\begin{Bmatrix} C_{km}^{x}(p) \\ C_{km}^{y}(p) \end{Bmatrix} + \begin{bmatrix} 0 & (G_y)_j/2 \\ (G_x)_j/2 & 0 \end{bmatrix}\sum_{m=1}^{M}U_{m-1}(\bar{x}_j)\begin{Bmatrix} C_{jm}^{x}(p) \\ C_{jm}^{y}(p) \end{Bmatrix} \tag{24a}$$

where $U_{m-1}(\bar{x}_j)$ is Chebyshev polynomial of the second kind and $V_j^{km}(\bar{x}_j)$ is

$$\left[V_j^{km}(\bar{x})_j\right] = \frac{1}{\pi}\int_{-1}^{1} \frac{\left[h_{jk}(\bar{r}_k,\bar{x}_j,p)\right]T_m(\bar{r}_k)}{\sqrt{1-\bar{r}_k^2}}\,\mathrm{d}\bar{r}_k. \tag{24b}$$

The crack open displacement $(u_{j-}^{*+}(\bar{x},p), v_{j-}^{*+}(\bar{x},p))$ can be evaluated from (8) and (9a) as

$$\left(u_{j-}^{*+}(\bar{x},p),v_{j-}^{*+}(\bar{x},p)\right) = h\int_{\bar{c}_j-\bar{a}_j}^{\bar{x}} \left(\phi_{xj}(\bar{r},p),\phi_{yj}(\bar{r},p)\right)\mathrm{d}r = \int_{-1}^{\bar{x}_j}\left(\varphi_{xj}(\bar{r}_j,p),\varphi_{yj}(\bar{r}_j,p)\right)\mathrm{d}\bar{r}_j. \tag{25a}$$

Substituting (21) and (22) into the above expression yields

$$\left(u_{j-}^{*+}(\bar{x},p),v_{j-}^{*+}(\bar{x},p)\right) = -a_j\sum_{m=1}^{M}\left(C_{jm}^{x}(p),\, C_{jm}^{y}(p)\right)\frac{\sin\left(m\arccos\bar{x}_j\right)}{m}, \quad |\bar{x}_j|<1. \tag{25b}$$

The traction boundary condition (2) require $(\sigma_j^*(x,p),\tau_j^*(x,p)) = (\sigma_{0j}^*(x,p),\tau_{0j}^*(x,p))$, this can be satisfied by

$$\int_{-1}^{1}\left[\sigma_j^*\left(\bar{a}_j\bar{x}_j+\bar{c}_j,p\right)-\sigma_{0j}^*\left(\bar{a}_j\bar{x}_j+\bar{c}_j,p\right)\right]\delta u_{j-}^{*+}\left(\bar{a}_j\bar{x}_j+\bar{c}_j,p\right)\mathrm{d}\bar{x}_j = 0$$

$$\int_{-1}^{1}\left[\tau_j^*\left(\bar{a}_j\bar{x}_j+\bar{c}_j,p\right)-\tau_{0j}^*\left(\bar{a}_j\bar{x}_j+\bar{c}_j,p\right)\right]\delta v_{j-}^{*+}\left(\bar{a}_j\bar{x}_j+\bar{c}_j,p\right)\mathrm{d}\bar{x}_j = 0. \tag{26}$$

In which δ is the variation sign. The integral eqn (20) can be recast into a system of linear algebraic equations by substituting (24a) and (25a) into (26)

$$\sum_{k=1}^{N-1}\sum_{m=1}^{M}\left[R_{jn}^{km}(p)\right]\begin{Bmatrix} C_{km}^{x}(p) \\ C_{km}^{y}(p)\end{Bmatrix} + \begin{bmatrix} 0 & \frac{\pi}{4}(G_y)_j \\ \frac{\pi}{4}(G_x)_j & 0\end{bmatrix}\begin{Bmatrix} C_{jm}^{x}(p) \\ C_{jm}^{y}(p)\end{Bmatrix} = \begin{Bmatrix} Q_{jn}^{y} \\ Q_{jn}^{x}\end{Bmatrix}$$

$$(j=1,2,\ldots,N-1 \quad n=1,2,\ldots,M) \tag{27a}$$

where

$$\left[R_{jn}^{km}(p)\right] = \int_{-1}^{1}\left[V_j^{km}\left(\bar{x}_j,p\right)\right]\sin\left(n\arccos\bar{x}_j\right)\mathrm{d}\bar{x}_j \tag{27b}$$

$$\left(Q_{jn}^{y} \quad Q_{jn}^{x}\right) = \int_{-1}^{1}\sigma_{0j}^*\left(\bar{a}_j\bar{x}_j+\bar{c}_j,p\right) \quad \tau_{0j}^*\left(\bar{a}_j\bar{x}_j+\bar{c}_j,p\right)\sin\left(n\arccos\bar{x}_j\right)\mathrm{d}\bar{x}_j. \tag{27c}$$

If the crack faces are loaded by concentrated shearing force $F_{xj}(t)$, and/or concentrated compressing force $F_{yj}(t)$ at the position of $\bar{x}_j = \bar{x}_{j0}$, we have

$$\left(Q_{jn}^{y}(p),\, Q_{jn}^{x}(p)\right) = \left(F_{yj}^*(p),\, F_{xj}^*(p)\right)\sin\left(n\arccos\bar{x}_{j0}\right). \tag{27d}$$

Once the coefficients $(C_{jm}^{x}(p),\, C_{jm}^{y}(p))$ are obtained, the numerical solution of the integral eqn (20) can

be calculated from (21) and (22). The displacements in the Laplace transform domain can be obtained from (24a) and (7).

Upon evaluating $(C^{x}_{jm}(p), C^{y}_{jm}(p))$ from (27a), it can be seen from (20)–(23) that the mode I and mode II stress intensity factors can be calculated as

$$(K^{*}_{\mathrm{I}})_j = (\sqrt{2[(c_j - a_j) - x]})_{x\to(c_j-a_j)} - \sigma^{*}_j(\bar{x}, p) = \frac{(G_y)_j\sqrt{a_j}}{2}\sum_{m=1}^{M}(-1)^m C^{y}_{jm}(p)$$

$$(K^{*}_{\mathrm{II}})_j = (\sqrt{2[(c_j - a_j) - x]})_{x\to(c_j-a_j)} - \tau^{*}_j(\bar{x}, p) = \frac{(G_x)_j\sqrt{a_j}}{2}\sum_{m=1}^{M}(-1)^m C^{x}_{jm}(p). \tag{28a}$$

For the left-hand side crack-tip and

$$(K^{*}_{\mathrm{I}})_j = (\sqrt{2[(c_j - a_j) - x]})_{x\to(c_j+a_j)} + \sigma^{*}_j(\bar{x}, p) = -\frac{(G_y)_j\sqrt{a_j}}{2}\sum_{m=1}^{M}C^{y}_{jm}(p)$$

$$(K^{*}_{\mathrm{II}})_j = (\sqrt{2[(c_j - a_j) - x]})_{x\to(c_j+a_j)} + \tau^{*}_j(\bar{x}, p) = -\frac{(G_x)_j\sqrt{a_j}}{2}\sum_{m=1}^{M}C^{x}_{jm}(p). \tag{28b}$$

For the right-hand side crack-tip.

After the solutions in the Laplace transform plane are obtained, we must use the inverse Laplace transform to get the solutions in the time domain. It is very difficult to make analytical inversions, and therefore numerical inversion is practical and useful. Although there are a number of numerical methods, the one used here is due to Miller and Guy (1966) which has been widely used in fracture dynamics (Fan, 1990; Jin and Noda, 1994).

Referring to the coefficients $(C^{0x}_{jm}(t), C^{0y}_{jm}(t))$ which denote the inverse Laplace transform of $(C^{x}_{jm}(p), C^{y}_{jm}(p))$ in the case of slowly loading, the problem is quasi-static, we may compute the energy release rates for the right-hand side crack-tip by virtual crack close technique

$$(G_{\mathrm{I}}(t))_j = \frac{1}{2}\lim_{\Delta\bar{a}\to 0}\frac{1}{\Delta\bar{a}}\int_0^{\Delta\bar{a}}\sigma_{0j}(\bar{x}+\bar{c}_j+\bar{a}_j, t)v^{+}_{j-}(\bar{x}+\bar{c}_j+\bar{a}_j-\Delta\bar{a}, t)\,\mathrm{d}\bar{x} = \frac{\pi(G_y)_j a_j}{8}\left[\sum_{m=1}^{M}C^{0y}_{jm}(t)\right]^2$$

$$(G_{\mathrm{II}}(t))_j = \frac{1}{2}\lim_{\Delta\bar{a}\to 0}\frac{1}{\Delta\bar{a}}\int_0^{\Delta\bar{a}}\tau_{0j}(\bar{x}+\bar{c}_j+\bar{a}_j, t)u^{+}_{j-}(\bar{x}+\bar{c}_j+\bar{a}_j-\Delta\bar{a}, t)\,\mathrm{d}\bar{x} = \frac{\pi(G_x)_j a_j}{8}\left[\sum_{m=1}^{M}C^{0x}_{jm}(t)\right]^2 \tag{29a}$$

and the energy release rates for the left-hand side crack-tip can be calculated as

$$(G_{\mathrm{I}}(t))_j = \frac{\pi(G_y)_j a_j}{8}\left[\sum_{m=1}^{M}(-1)^m C^{0y}_{jm}(t)\right]^2, \quad (G_{\mathrm{II}}(t))_j = \frac{\pi(G_x)_j a_j}{8}\left[\sum_{m=1}^{M}(-1)^m C^{0x}_{jm}(t)\right]^2. \tag{29b}$$

The relationship between the stress intensity factor and energy release rate can be evaluated from (28) and (29)

$$(G_{\mathrm{I}}(t))_j = \frac{\pi}{2(G_y)_j}(K_{\mathrm{I}}(t))_j^2 \quad (G_{\mathrm{II}}(t))_j = \frac{\pi}{2(G_x)_j}(K_{\mathrm{II}}(t))_j^2. \tag{30a}$$

The total energy release rate is

$$(G(t))_j = (G_{\mathrm{I}}(t))_j + (G_{\mathrm{II}}(t))_j = \frac{\pi}{2}\left(\frac{(K_{\mathrm{I}}(t))_j^2}{(G_y)_j} + \frac{(K_{\mathrm{II}}(t))_j^2}{(G_x)_j}\right). \tag{30b}$$

5. Numerical examples and discussion

The approach outlined in the foregoing is employed to investigate the response of three different specimens with functionally graded layer. The specimen geometry and crack position are shown in Fig. 2. The first specimen is a functionally graded material with a crack of length $2a = h$ in the center, and the second, a metal-ceramic joint with functionally graded interlayer, each of the interfaces contains a crack of equal length. The third specimen is a metal substrate/functionally graded film structure with a fixed substrate thickness $h_m = 4a$.

The functionally graded layer are metal/ceramic composite. The metal phase and ceramic phase are taken as A1 and $A1_2O_3$. The properties of metal and ceramic are

$$\text{Al:} \quad E_m = 69\ \text{Gpa} \quad \nu_m = 0.33 \quad \rho_m = 2700\ \text{Kg/m}^3 \tag{31a}$$

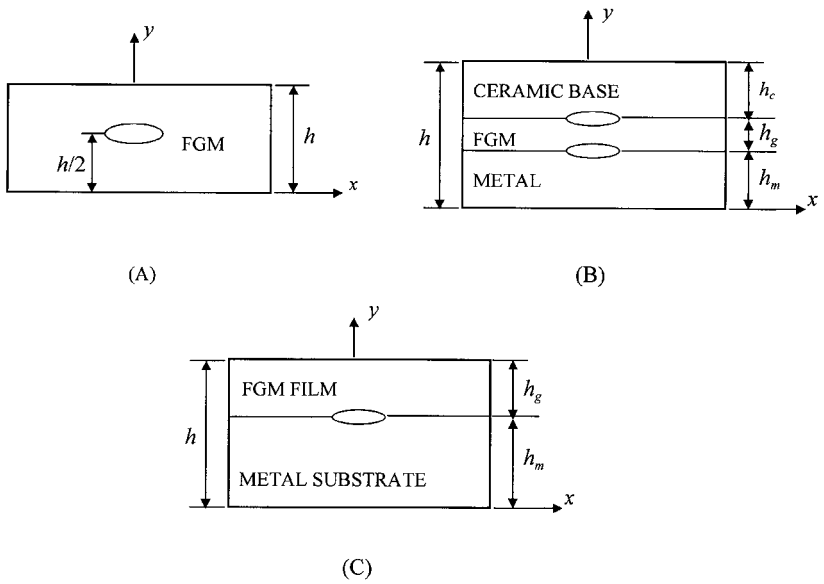

Fig. 2. Specimens geometry considered, (A) a functionally graded material with a crack of length $2a = h$, (B) a metal-ceramic joint with functionally graded interlayer, the dimension is fixed as $h_c = h_g = h_m$, and (C) a substrate-film structure with a crack of a length $2a = 0.25h_m$ in the interface.

$$Al_2O_3: \quad E_c = 300\ \text{Gpa} \quad \nu_c = 0.27 \quad \rho_c = 3900\ \text{Kg/m}^3 \tag{31b}$$

in which E, ρ, ν are elastic module, Poision's ratio and mass density, the subscript m and c denote metal phase and ceramic phase, respectively. Using the properties given above, one can calculate the shearing wave velocity C_m in metal A1 to be 98 m/s. In the analysis, the graded regions were treated as a series of perfectly bonded composite layers, each layer being assigned slightly different material properties (however, the two layers adjacent to the cracked plane are taken to have the same material properties). At any position y in the functionally graded ceramic/metal layer, the local volume fraction of metal is assumed to be $g(y)$ which can be used to characterize the coating gradation, $g(y)$ can be any non-singular, non-negative function of y. To gain insight into the effect of material gradation on the dynamic stress intensity factors (SIFs) and strain energy release rates (SERRs), it is assumed that the local volume fraction of metal $g(y)$ obeys a power-law type relation

$$g(y) = \begin{cases} \dfrac{0.5}{1-0.5^q}\left[1-\left(\dfrac{y}{h}\right)^q\right] & q \geqslant 1 \\ 1-\dfrac{0.5}{0.5^q}\left(\dfrac{y}{h}\right)^q & q < 1 \end{cases} \tag{32a}$$

for functionally graded material specimen (A), and

$$g(y) = 1-\left(\frac{y-h_m}{h_g}\right)^{1/q} \tag{32b}$$

for joint specimen (B) and substrate-film specimen (C).

In the above expression q is known as a gradient exponent or non-homogeneity parameter. From (32a) one can see that for the functionally graded material specimen (a), the local volume fraction of metal is always 50% at the position $y = h/2$ regardless of the q value. The expression (32b) implies that the functionally graded layer has pure metal at the bottom surface and pure ceramic at the upper

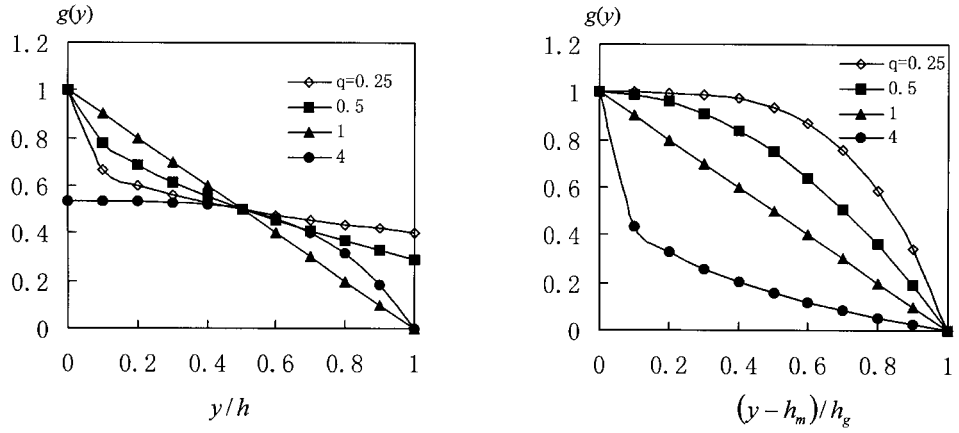

Fig. 3. Composition gradients for several values of the gradient exponent q.

surface of the layer. The composite profile for q values of 0.25, 0.5, 1, 2, and 4 are shown in Fig. 3. It is clear that the total volume fraction of the functionally graded layer is metal rich for $q < 1$ and ceramic rich for $q > 1$.

Relating $g(y)$ to the local value of the 'average' material properties of the composite is not a trivial matter. To keep things simple, we choose an elementary 'Law-of-mixtures' model, i.e.

$$E(y) = g(y)E_m + \big(1 - g(y)\big)E_c \quad v(y) = g(y)v_m + \big(1 - g(y)\big)v_c \quad \rho(y) = g(y)\rho_m + \big(1 - g(y)\big)\rho_c. \tag{33}$$

The rule expressed by (33) being known as a Voigt-type estimate. A more realistic expression would be based on the micromechanics of composite. For example, micromechanics based 'Mori–Tanaka' model have been presented (Mori, 1987).

For the purpose of numerical illustration, assume that a sudden uniform stress is applied on the crack

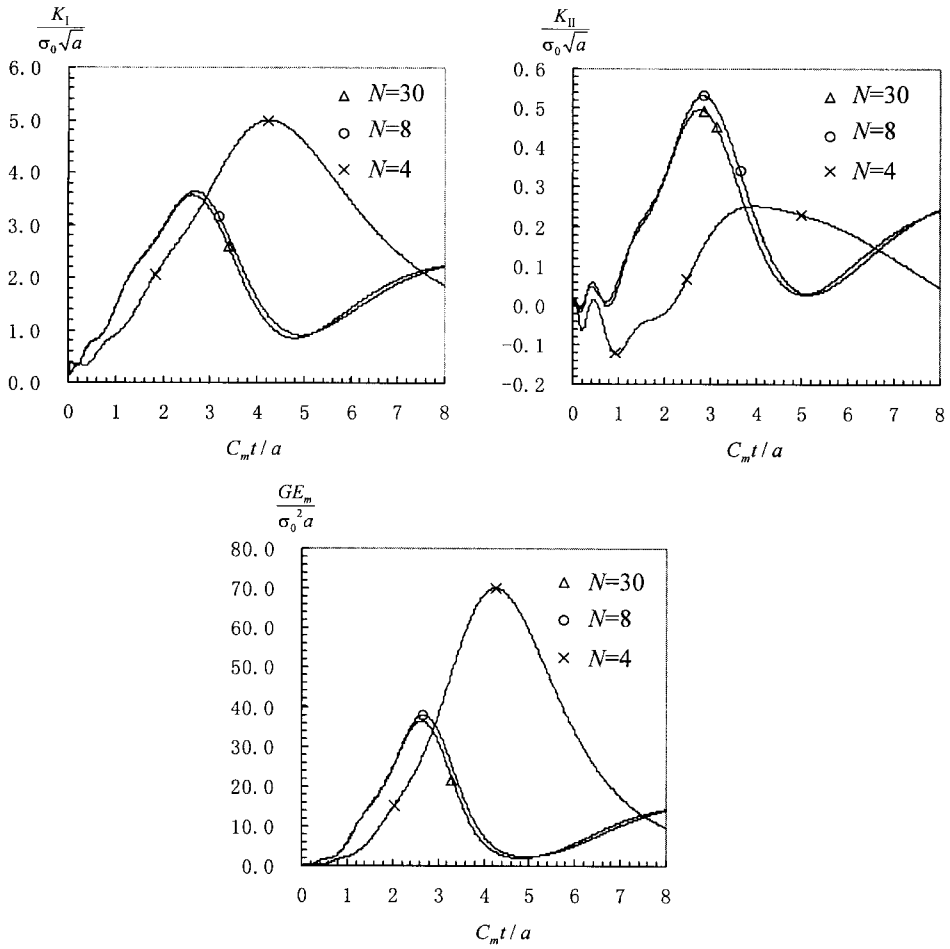

Fig. 4. The influence of divided layers number N on SIFs and SERRs for specimen (A), the gradient exponent q is fixed as 1.

faces. The related integrals are evaluated by using the Gauss-Chebyshev formulae. The calculated SIFs and SERRs for the right-hand side crack-tip are carried out for three specimens.

5.1. Specimen (A), a functionally graded material

Specimen (A) is a functionally graded material with a crack of length $2a = h$ in the center. The load condition is a sudden uniform compressing stress σ_0 on the crack faces. In order to simulate material gradation along thickness direction, the material was divided into some layers (say N layers) in that direction. The influences of layers number N on SIFs and SERRs are depicted in Fig. 4 for a fixed gradient exponent $q = 1$. It is found that at any time of t SIFs and SERRs tend to converge to a steady value as N becomes sufficiently large, this indicates that we can use the laminated composite plate model to simulate the material non-homogeneity in the thickness direction. Hence, in the following, the divided

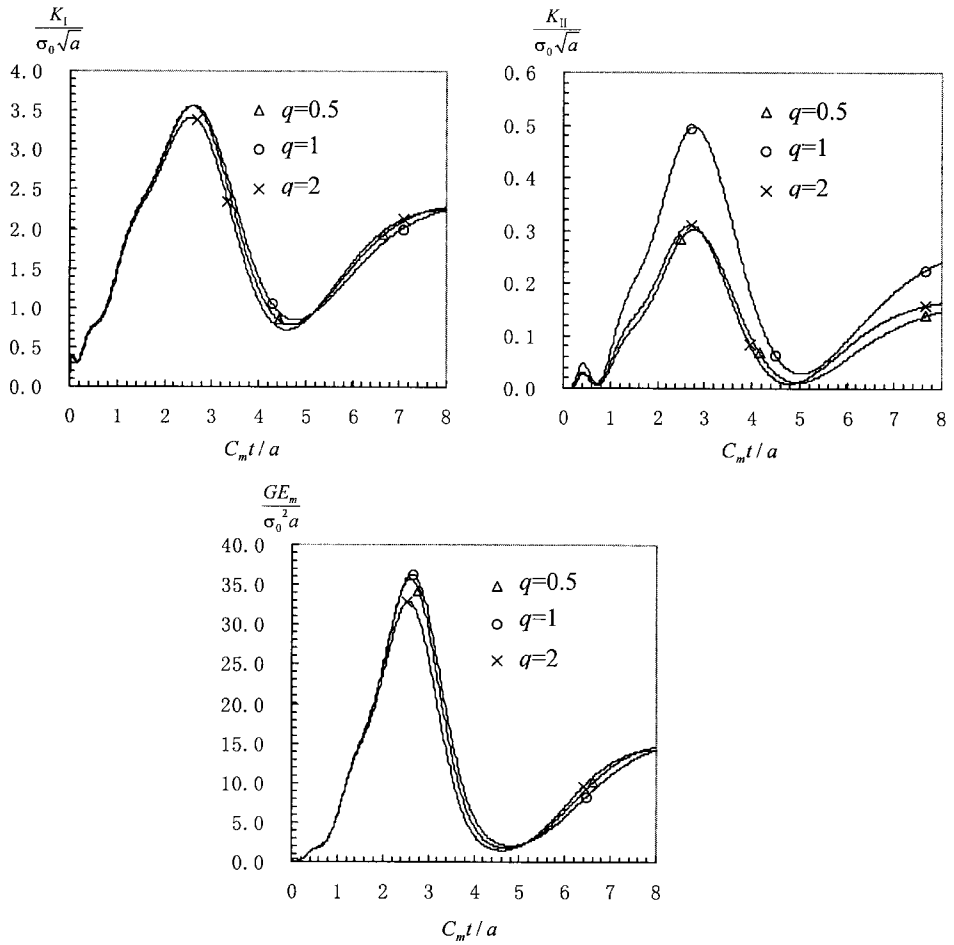

Fig. 5. The effect of gradient exponent, q, on SIFs and SERRs for specimen (A).

layers number N is selected to be large enough for obtaining the solutions to the defined problem with a required degree of accuracy.

Displayed in Fig. 5 is the influence of gradient exponent q on the non-dimensional SIFs and SERRs at different time t. The following facts can be found from these figures. Firstly, under the range of q considered, SIF tends to rise quickly as time increases. All the curves reach a peak and then decrease in

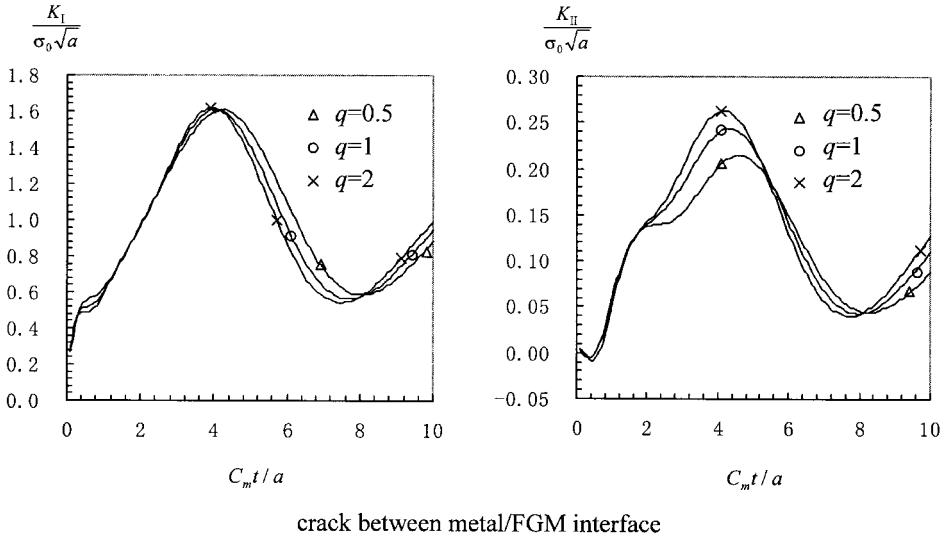

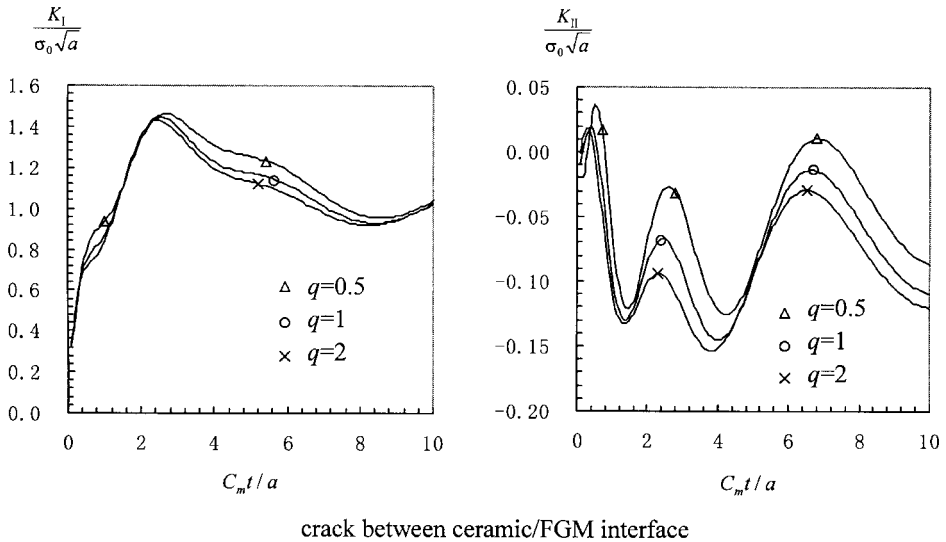

Fig. 6. The effect of gradient exponent, q, on SIFs induced by uniform compressing stress σ_0, the dimensions are fixed as $2a = h_c = h_g = h_m$.

magnitude. Secondly, the peak mode II SIFs and SERRs are more pronounced for higher q than for lower q. Thirdly, although the geometry of the material is symmetrical with respect to the $y = h/2$ plane, due to material non-homogeneity the stress state around the crack tips is one of mixed mode. It is also found that the mode I SIFs is not highly sensitive to q values, the differences were more significant for mode II stress intensity factors.

5.2. Specimen (B), a metal–ceramic joint with a functionally graded interlayer

The joint contains a metal base and a ceramic base bonded by a functionally graded interlayer as shown in Fig. 2(B). The load conditions are suddenly applying uniform compressing stress σ_0 on the crack faces. Since the interaction between the cracks, the influences of gradient function exponent q and interlayer thickness hg on SIFs and SERRs are very complicated. Fig. 6 illustrates the effects of varying the gradient function exponent q, for a fixed crack length $2a = h_c = h_g = h_m$. Within the range of exponents examined, the influence of q is unimportant. Displayed in Fig. 7 is the energy release rate with time for different gradient exponents. Note that for this joint specimen with FGM interlayer the effect of the non-homogeneity constraint q on the peak energy release rate is negligible.

Again let $h_c = h_m = h_g$. Figs. 8 and 9 show the effect of joint thickness on SIFs and SERRs calculated using a linear compositional profile ($q = 1.0$). Results are displayed for K_I, K_{II} and G assuming interlayer thickness of $h_g = 1.5a$, $h_g = 2a$, and $h_g = 3a$. Within the range of h_g examined, it seems that as h_g increase the peak values of SIFs and SERRs decrease. The same trends can also be seen from Figs. 10 and 11 for steady SIFs and SERRs. These figures indicate that the stress intensity factors and strain energy release rate are monotonically decreasing functions of h_g, this is due to the fact that as h_g increased the global stiffness of the medium is also increased. Furthermore, one can see that for this two crack problem, at the right crack tip ($x = +a$), K_{II} are positive for crack between metal/

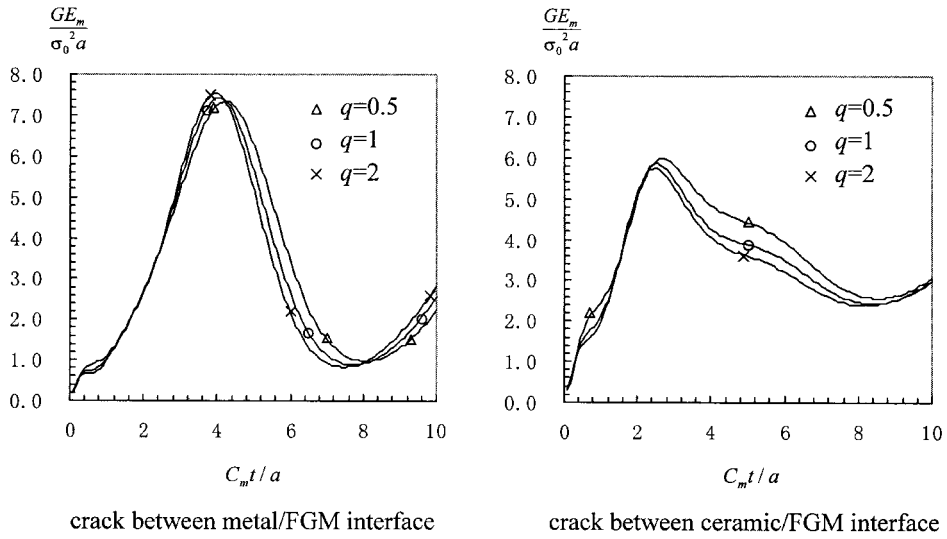

Fig. 7. The effect of gradient exponent, q, on SERRs induced by uniform compressing stress σ_0, the dimensions are fixed as $2a = h_c = h_g = h_m$.

FGM interface and negative for crack between ceramic/FGM interface, this indicates that the value of K_{II} are strongly dependent on the crack position.

5.3. Specimen (C), substrate-film structure

The specimen (C) contains a metal substrate and a functionally graded metal/ceramic film. The

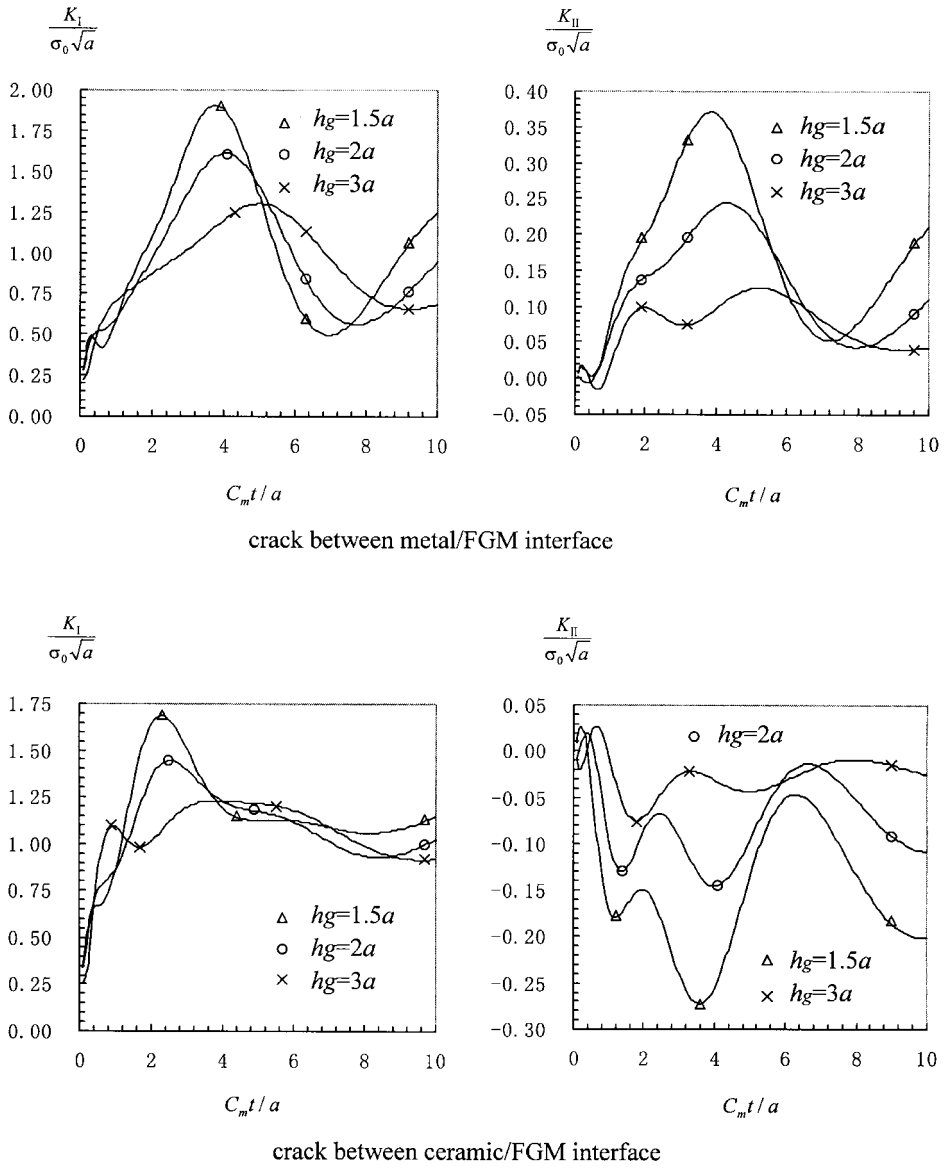

Fig. 8. The effect of joint thickness on dynamic SIFs induced by uniform compressing stress σ_0 with a fixed gradient exponent ($q = 1.0$).

substrate thickness is taken to be equal to two times of crack length. The load condition is suddenly applying uniform compressing stress σ_0 on crack faces. Figs. 12 and 13 display the influence of varying gradient exponent q on stress intensity factors and strain energy release rates, respectively. The assumed film thickness h_g is $0.25h_m$. Noting that within the range of exponents examined, as gradient exponent q increases the peak SIFs K_I (the dominant stress intensity factor) and SERRs decrease, this is due to the fact that as the gradient exponent q increases the stiffness of the film also increases.

Illustrated in Figs. 14 and 15 are the effects of the film thickness on the dynamic SIFs and SERRs, respectively. All the curves are computed using a linear compositional profile ($q = 1.0$). The assumed film thickness is $0.75h_m$, $0.5h_m$ and $0.25h_m$. It is found that for small film thickness, increasing the thickness of the film reduces the dynamic mode I SIFs and SERRs. But when the thickness of the film is large enough the influence of h_g is negligible.

Figs. 16 and 17 show the influence of film thickness on static SIFs and SERRs. The following facts can be found from these figures. Firstly, for small film thickness, the mode I SIFs (the dominant stress intensity factor) and SERRs are monotonically decreased functions of h_g, while for larger film thickness, the influence of h_g is negligible. Secondly, as $h_g \to 0$, K_I, K_{II} and G are unbounded, as $h_g \to \infty$, K_I, K_{II} and G approach to some fixed values, since the substrate thicknesses are not infinite, the fixed values are not one for K_I and zero for K_{II}. Thirdly, regardless of the fact that in the neighborhood of the crack the stiffness of the medium increase in the $+y$ direction, for small film thickness, the stiffness of film is smaller than that of the substrate and consequently the mode II stress intensity factors K_{II} at the right crack tip are negative, while for larger film thickness the stiffness of the film is larger than that of the substrate and consequently the mode II stress intensity factors K_{II} at the right crack tip become positive.

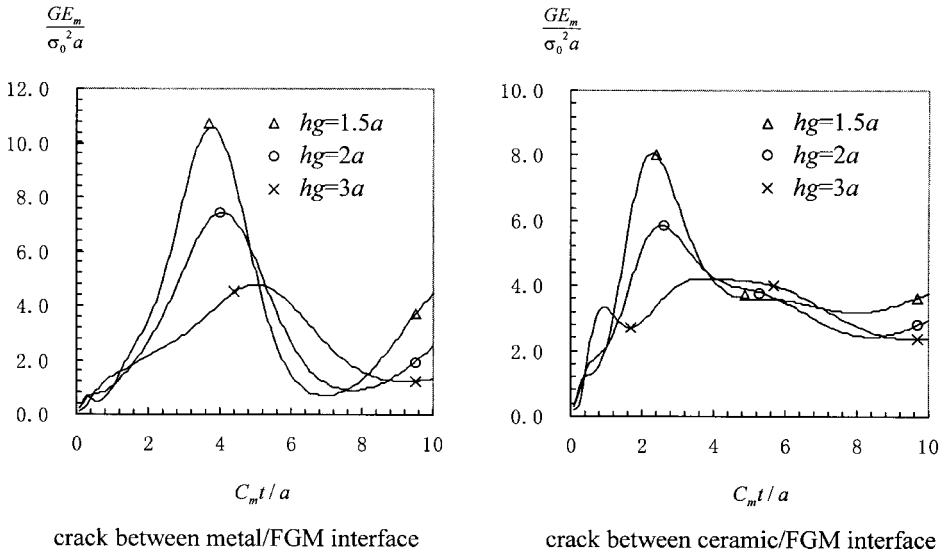

Fig. 9. The effect of joint thickness on dynamic SERRs induced by uniform compressing stress σ_0, with a fixed gradient exponent ($q = 1.0$).

6. Summary and conclusions

Non-homogeneous composite materials are potentially very attractive for a number of applications. Many researchers, especially Erdogan and his coworkers, have carried out mechanics analyses for the fracture behavior of these materials. The problem considered in this paper is that the response of a non-homogeneous composite materials plate containing some non-collinear cracks subjected to dynamic

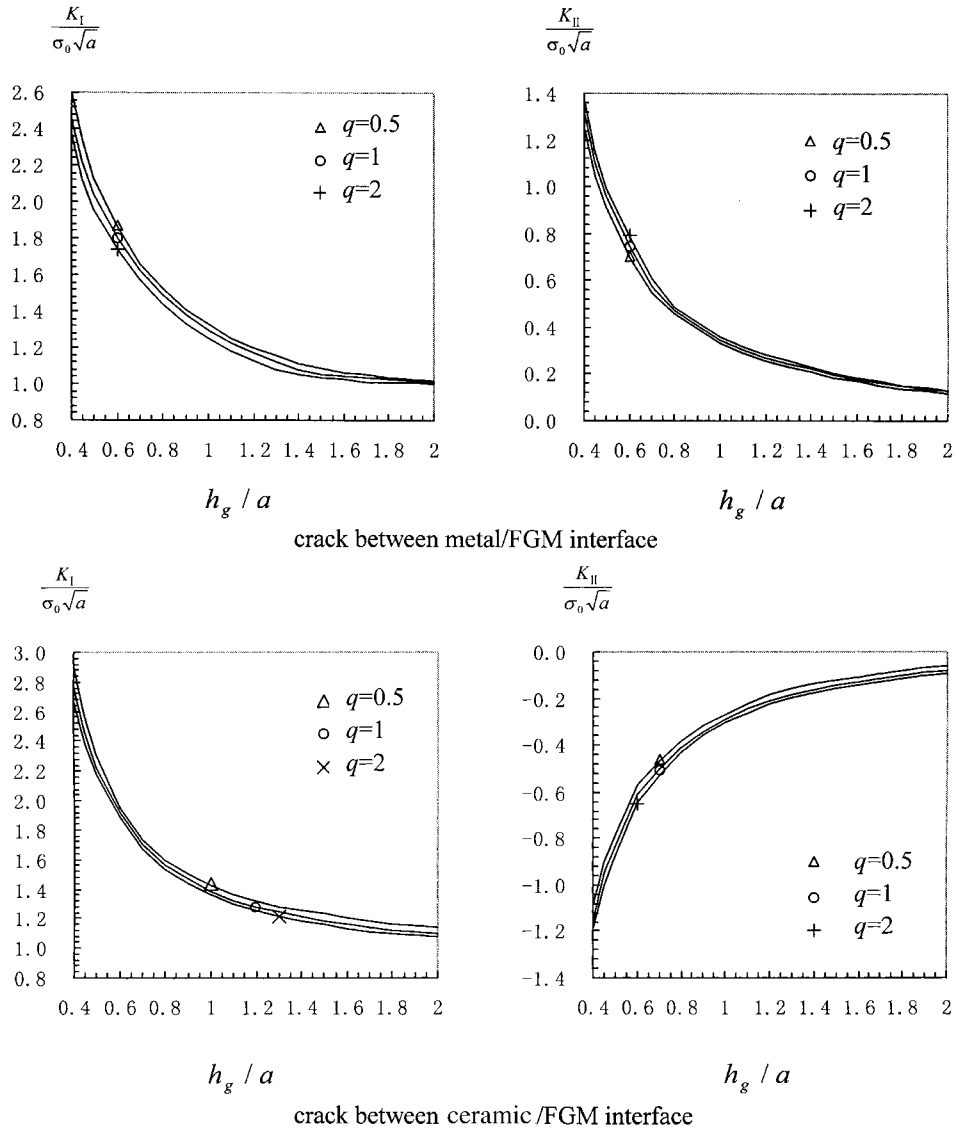

Fig. 10. The effect of joint thickness on steady state SIFs induced by uniform compressing stress σ_0, for different gradient exponent q.

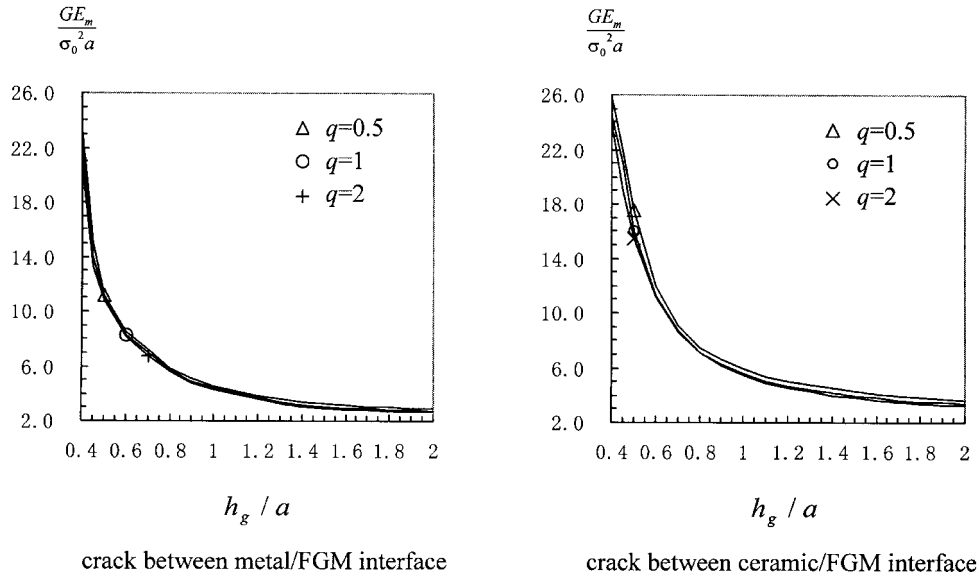

Fig. 11. The effect of joint thickness on steady state SERRs induced by uniform compressing stress σ_0, for different gradient exponent q.

loading. In the analysis, the elastic region is divided into a number of layers of infinite length. The material properties are taken to be constants for each layer (however, the two layers adjacent to the cracked plane are taken to have the same material properties). Three different cracked specimens, a functionally graded material, a metal–ceramic joint with functionally graded interlayer, and a metal substrate/functionally graded film structure are presented as numerical illustrations. From the numerical examples, we found that the computing time is mainly dependent on the crack number, so we can divide

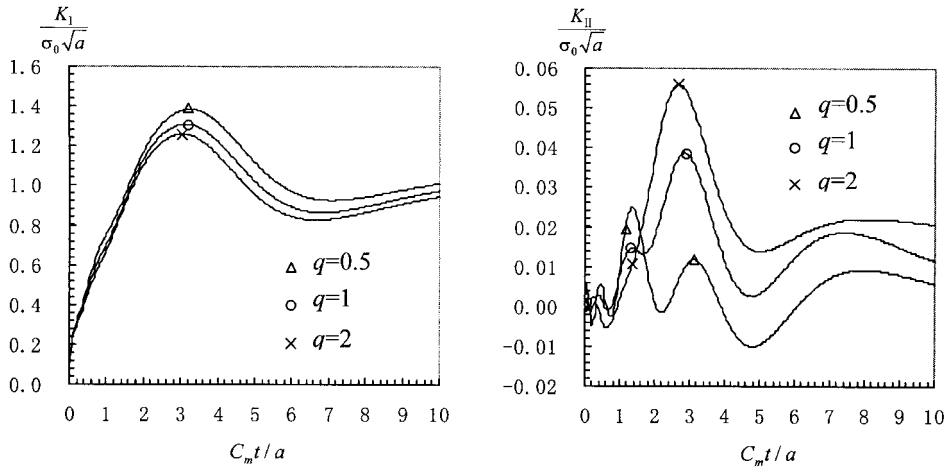

Fig. 12. The effect of gradient exponent, q, on SIFs for specimen (C).

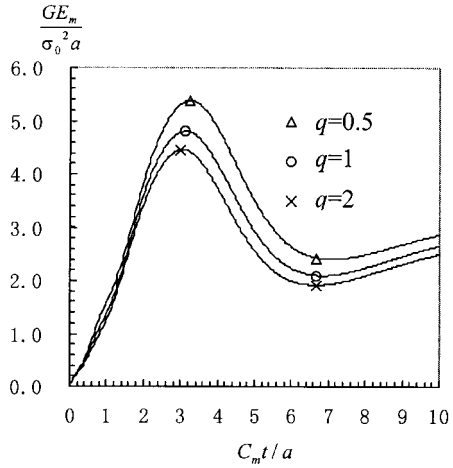

Fig. 13. The effect of gradient exponent, q, on SERRs for specimen (C).

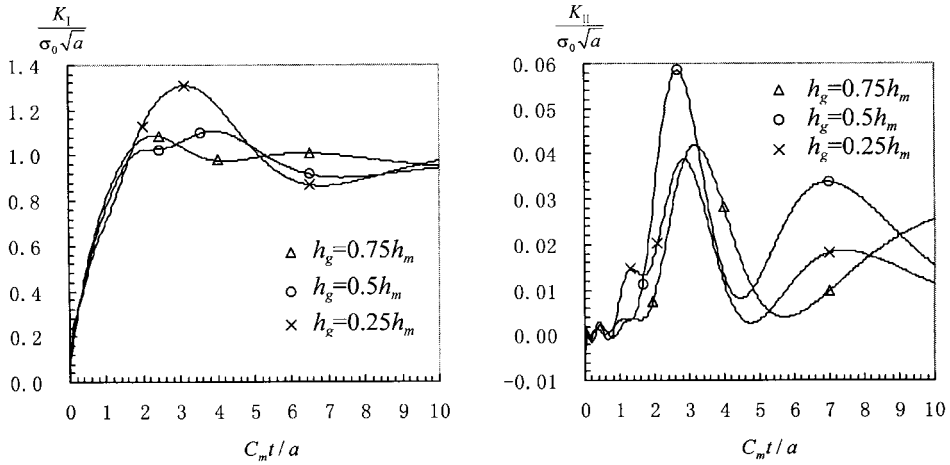

Fig. 14. The effect of film thickness, h_g, on dynamic SIFs for specimen (C) with a fixed gradient exponent (q = 1.0).

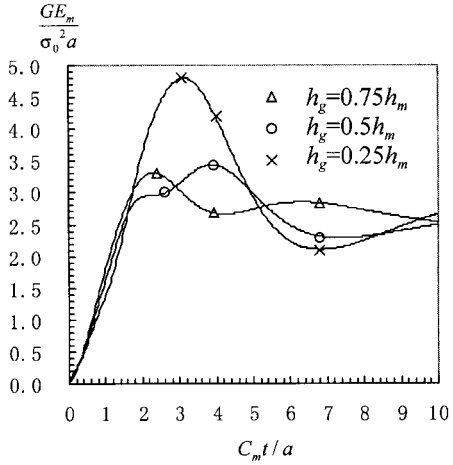

Fig. 15. The effect of film thickness, h_g, on dynamic SERRs for specimen (C) with a fixed gradient exponent (q = 1.0).

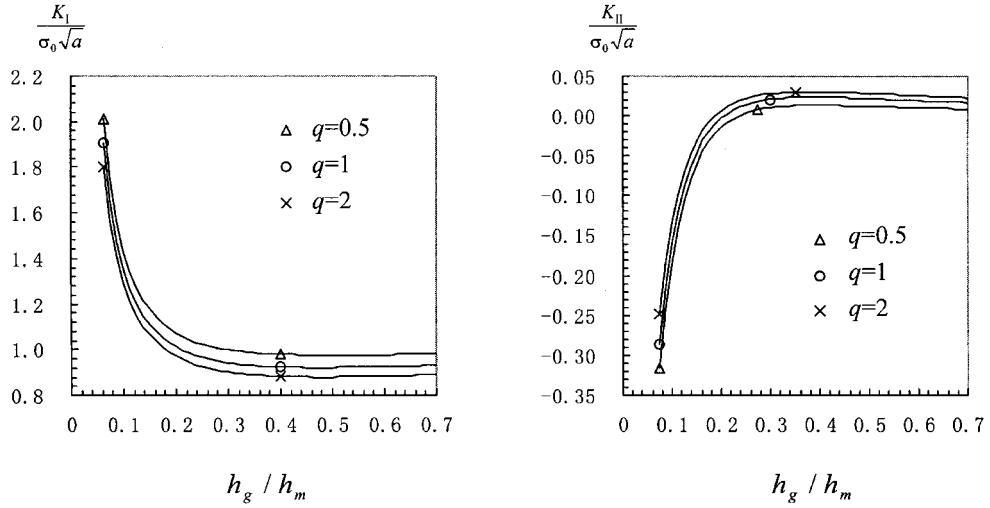

Fig. 16. The effect of film thickness, h_g, on steady state SIFs, for different gradient exponent q.

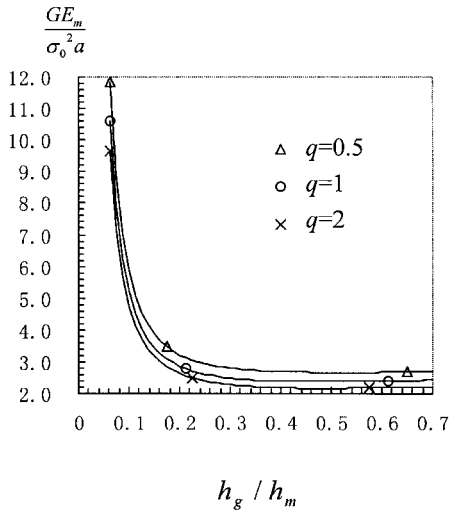

Fig. 17. The effect of film thickness, h_g, on steady state SERRs, for different gradient exponent q.

the material into a larger number of layers to simulate material gradient. Differing from the existing works reported in literature, the present method can be used for arbitrarily varying material properties through thickness direction and the crack number can be larger than one.

References

Ashbaugh, N.E., 1973. Stress in laminated composites containing a broken layer. J. Appl. Mech. 40, 533–540.
Chen, E.P., Sih, G.C., 1971. Interfacial delamination of a layered composite under antiplane strain. J. Comp. Mat. 5, 12–23.

Delale, F., Erdogan, F., 1988a. On the mechanical modeling of the interfacial region in bonded half-planes. J. App. Mech. 55, 317–324.

Delale, F., Erdogan, F., 1988b. Interface crack in a nonhomogeneous elastic medium. Int. J. Engng Sci. 26, 559–568.

Erdogan, F., 1985. The crack problem for a bonded nonhomogeneous material under antiplane shear loading. J. Appl. Mech. 52, 823–825.

Fan, T.Y., 1990. Introduction to Fracture Dynamic. Beijing Institute of Technology Press, Beijing.

Gradshteyn, I.S., Ryzhik, I.M., 1965. Tables of Integrals, Series and Products. Academic Press, New York.

Hata, T., 1985. Thermal stress in a nonhomogeneous semi-infinite elastic solid under steady distribution of temperature. Transaction of the Japan Society of Mechanical Engineers (A) 51, 1789–1795.

Jin, Z.H., Noda, N., 1994. Transient thermal stress intensity factors for a functionally gradient material. Int. J. Solids Structures 31, 203–218.

Kaizu, K., Suzuki, Y., Tanimura, S., 1991. Numerical analysis of stress wave propagation in a circular tube made of functionally gradient materials. Transaction of the Japan Society of Mechanical Engineers (A) 57, 143–147.

Miller, M.K., Guy, W.T., 1966. Numerical inversion of the Laplace transform by use of Jacobi polynomials. SIAM J. Numer. Anal. 3, 624–635.

Mori, T., 1987. Micromechanics of Defects in Solids, 2nd ed. Nijhoff, Martinus, Dordrecht.

Muskhelishvili, N.I., 1953. Singular Integral Equations. Noordhoff, Groningen, The Netherlands.

Ozturk, M., Erdogan, F., 1993. The antisymmetric crack problem in a nonhomogeneous medium. J. Appl. Mech. 60, 406–413.

Ozturk, M., Erdogan, F., 1995. An axisymmetric crack in bonded materials with a nonhomogeneous interfacial zone under torsion. J. Appl. Mech. 62, 116–125.

Ozturk, M., Erdogan, F., 1996. Axisymmetric crack problem in bonded materials with a graded interfacial region. Int. J. Solids Structures 33, 193–219.

Ryvkin, M., 1996. Mode III crack in a laminated medium. Int. J. Solids Structures 33, 3611–3625.

Slepyan, L., 1974. Crack in layered medium. In: Selected Problems of Applied Mechanics. Viniti, Moscow, pp. 557–564 (in Russian).

Williams, M.L., 1959. The stress around a fault of crack in dissimilar media. Bull. Seismological Society of America 49, 199–204.

Zuiker, J.R., 1995. Functionally graded materials: choice of micromechanics model and limitations in property variation. Comp. Engng 5, 807–819.